Fundamental Bounds on the Precision of Classical Phase Microscopes

Dorian Bouchet[1] Jonathan Dong,[2] Dante Maestre,[3,4] and Thomas Juffmann[3,4,*]

[1] *Nanophotonics, Debye Institute for Nanomaterials Science and Center for Extreme Matter and Emergent Phenomena, Utrecht University, P.O. Box 80000, 3508 TA Utrecht, Netherlands*

[2] *Laboratoire Kastler Brossel, ENS-Université PSL, CNRS, Sorbonne Université, Collége de France, 24 rue Lhomond, 75005 Paris, France*

[3] *Faculty of Physics, University of Vienna, VCQ, A-1090 Vienna, Austria*

[4] *Max Perutz Laboratories, Department of Structural and Computational Biology, University of Vienna, A-1030 Vienna, Austria*

A wide variety of imaging systems have been designed to measure phase variations, with applications from physics to biology and medicine. In this work, we theoretically compare the precision of phase estimations achievable with classical phase microscopy techniques, operated at the shot-noise limit. We show how the Cramér-Rao bound is calculated for any linear optical system, including phase-contrast microscopy, phase-shifting holography, spatial light interference microscopy, and local optimization of wavefronts for phase imaging. Through these examples, we demonstrate how this general framework can be applied for the design and optimization of classical phase microscopes. Our results show that wavefront shaping is required to design phase microscopes with optimal phase precision.

I. INTRODUCTION

Phase microscopy enables precise measurements of optical path length differences [1–4]. All phase images are constructed from a finite number of detected photons. This number can be limited by technological constraints, such as the source power or the dynamic range of the detector. The maximum photon flux can also be dictated by specimen damage, e.g., in dispersive imaging of ultracold atoms where inelastic scattering and elastic recoil lead to atom loss and heating [5,6], respectively. Another example is the imaging of biological structures with ultraviolet radiation [7,8], where inelastic channels lead to sample damage. In such applications, it is therefore crucial to maximize the information retrieved per photon.

Nowadays, many different variations of phase microscopes exist [3], all of which convert optical path length differences into detectable intensity variations. The Cramér-Rao bound (CRB) allows quantifying the precision that can be achieved with any given phase microscopy technique, as it imposes a lower limit to the precision that can be achieved in the estimation of parameters from noisy data [9,10]. Such quantitative analysis of the achievable estimation precision is of great importance in many fields, be it in fluorescence microscopy regarding particle localization precision [11–13], in interferometric scattering microscopy regarding the possibility to detect and characterize single proteins without labeling them [14,15], or in electron microscopy regarding particle structure determination [16]. In the context of phase microscopy, several recent studies have focused on the question of how to increase the precision of phase estimations using quantum correlations of the probe light in phase microscopy [17,18]. However, quantum enhanced schemes are difficult to realize experimentally, and common phase microscopes do not even reach the optimum CRB achievable with uncorrelated light.

Here, we expose the experimental conditions necessary to reach the optimal precision on phase estimations based on shot-noise-limited measurements. Via a Cramér-Rao analysis, we demonstrate that common phase microscopy techniques fall short of this limit because they are not ideal for the specimens under study. Additionally, we show that wavefront-shaping techniques, which recently found several applications in phase microscopy [19–23], can be used to recover the optimal estimation precision for any given phase sample. The manuscript is organized as follows. In Sec. II, we derive fundamental bounds based on the Cramér-Rao inequality for the precision of any classical linear phase microscope. In Sec. III, we discuss how to reach this bound in the case of an external reference, which requires wavefront shaping for strong phase objects. In Sec. IV, we show how this framework also applies to imaging systems with an internal reference.

_____

*Corresponding author. thomas.juffmann@univie.ac.at

II. THEORETICAL FRAMEWORK

A. General model for phase microscopes

We consider a general model in which coherent light propagates through a phase sample, so that local phase shifts induced by the object are imprinted in the transmitted wavefront. By partitioning our region of interest in p small surfaces of area S_a, the average number of photons passing through the jth area within a time Δt is then given by $n_j = \Delta t |E_j^{\mathrm{obj}}|^2$, where $E_j^{\mathrm{obj}} = \mathcal{A}_j e^{i\phi_j}$ denotes the complex field associated with this area. Note that this definition of the field differs from the classical definition of the complex electric field (in SI units) by a factor $\sqrt{(n_{\mathrm{obj}}\epsilon_0 c S_a)/(2\hbar\omega)}$, where n_{obj} is the object refractive index, ϵ_0 is the vacuum permittivity, c is the speed of light in vacuum, ω is the photon angular frequency, and $\hbar$ is the reduced Planck constant.

To estimate the phase values $\phi = (\phi_1, \dots, \phi_p)$, we use a linear optical system characterized by an operator $H \in \mathbb{C}^{d \times p}$ whose elements are noted $h_{kj} = |h_{kj}|e^{i\beta_{kj}}$. With these notations, the average intensity image on the camera is

$$I^{\mathrm{det}} = |HE^{\mathrm{obj}} + E^{\mathrm{ref}}|^2, \qquad (1)$$

where we introduced an optional external reference field $E^{\mathrm{ref}} \in \mathbb{C}^d$.

Let us consider that the data measured by the camera are described by a d-dimensional random variable X characterized by a joint density probability function $p(X; \phi)$. The variance of any unbiased estimator $\hat{\phi}(X)$ of ϕ must satisfy the Cramér-Rao inequality [9], which is expressed by

$$\mathrm{Var}(\hat{\phi}_j) \geq [\mathcal{J}^{-1}(\phi)]_{jj}, \qquad (2)$$

where Var is the variance operator and $\mathcal{J}(\phi)$ the Fisher information matrix defined by

$$[\mathcal{J}(\phi)]_{ij} = E\left[\left(\frac{\partial \ln p(X; \phi)}{\partial \phi_i}\right)\left(\frac{\partial \ln p(X; \phi)}{\partial \phi_j}\right)\right], \quad (3)$$

with E the expectation operator acting over noise fluctuations. Maximum-likelihood estimators are known to saturate this inequality in the asymptotic limit [9]. Consequently, measuring a large number of photons is a sufficient condition for this inequality to be saturable.

Since the Fisher information matrix is positive semidefinite, we can also write the inequality

$$[\mathcal{J}^{-1}(\phi)]_{jj} \geq [\mathcal{J}(\phi)]_{jj}^{-1}. \qquad (4)$$

This inequality, which results from properties of the Schur complement, highlights the central role played by the diagonal elements of the Fisher information matrix upon the precision of estimations. It is in fact saturated when the Fisher information matrix is diagonal, which corresponds to the case in which the estimation of ϕ_j is not influenced by an imperfect knowledge of all other parameters. Alternatively, this also corresponds to the case in which one seeks to estimate a given parameter ϕ_j assuming that the values of all other parameters are known.

B. Fisher information in the shot-noise limit

We now assume that shot noise, i.e., the detection statistics due to the quantized nature of light, is the main source of noise, and that we can neglect mechanical vibrations, readout noise, dark currents, and other sources of noise. Considering an integration time Δt and assuming that the values measured by all camera pixels are statistically independent, the probability density function $p(X; \theta)$ simplifies to

$$p(X; \theta) = \prod_{k=1}^{d} \frac{e^{-\Delta t I_k^{\mathrm{det}}}(\Delta t I_k^{\mathrm{det}})^{X_k}}{X_k!}. \qquad (5)$$

Substituting Eq. (5) into Eq. (3) yields

$$[\mathcal{J}(\phi)]_{ij} = \Delta t \sum_{k=1}^{d} \frac{1}{I_k^{\mathrm{det}}}\left(\frac{\partial I_k^{\mathrm{det}}}{\partial \phi_i}\right)\left(\frac{\partial I_k^{\mathrm{det}}}{\partial \phi_j}\right). \qquad (6)$$

Using the equality $I^{\mathrm{det}} = |E^{\mathrm{det}}|^2$ to express the derivative of the intensity I_k^{det} with respect to ϕ_j, we obtain

$$\frac{\partial I_k^{\mathrm{det}}}{\partial \phi_j} = -2\,\mathrm{Im}[(E_k^{\mathrm{det}})^* h_{kj} E_j^{\mathrm{obj}}]. \qquad (7)$$

Writing $E_k^{\mathrm{det}} = |E_k^{\mathrm{det}}|e^{i\alpha_k}$, the diagonal elements of the Fisher information matrix are expressed by

$$[\mathcal{J}(\phi)]_{jj} = 4n_j \sum_{k=1}^{d} |h_{kj}|^2 \sin^2(\phi_j + \beta_{kj} - \alpha_k). \qquad (8)$$

Equation (8) is maximized if two conditions are satisfied. First, we have $\sin^2(\phi_j + \beta_{kj} - \alpha_k) \leq 1$, with the equality holding if the following phase-matching condition is fulfilled:

$$\phi_j + \beta_{kj} - \alpha_k = \pi/2 + m\pi \qquad (9)$$

with m being any integer. The condition must hold for all k, j for which $n_j|h_{kj}|2 \neq 0$. Second, we can remark that energy conservation imposes a condition on H. Indeed, the total intensity of the object field is $\|E^{\mathrm{obj}}\|^2$, and becomes after propagation through the optical system $\|HE^{\mathrm{obj}}\|^2 = E^{\mathrm{obj}\dagger}H^\dagger H E^{\mathrm{obj}}$. In general, since the passive linear optical system can only decrease the transmitted energy, the inequality $\|HE^{\mathrm{obj}}\|^2 \leq \|E^{\mathrm{obj}}\|^2$ is always satisfied. Energy

conservation thus imposes that $\sum_k |h_{kj}|^2 \leq 1$, with the equality holding if energy is conserved and H is a unitary matrix. Hence, we obtain the inequality

$$[\mathcal{J}(\phi)]_{jj} \leq 4n_j, \qquad (10)$$

which is saturated if H is unitary and if the phase-matching condition expressed by Eq. (9) is satisfied.

To summarize the results from this section, we can use Eqs. (2), (4), and (10) to write the following chain of inequalities:

$$\mathrm{Var}(\hat{\phi}_j) \geq [\mathcal{J}^{-1}(\phi)]_{jj} \geq [\mathcal{J}(\phi)]_{jj}^{-1} \geq \frac{1}{4n_j}. \qquad (11)$$

In order to design a phase microscope that reaches this fundamental bound, one needs to saturate all the inequalities in Eq. (11), leading to several conditions. The first inequality is saturated asymptotically with maximum-likelihood estimators [9], which implies that this inequality can be saturated when $\Delta t I_k^{\mathrm{det}} \gg 1$ over the whole field of view (FOV). To saturate the second inequality, the Fisher information matrix needs to be diagonal, such that no correlation exists in the estimated values of different parameters. For the last inequality to be saturated, two additional conditions must be satisfied. First, the optical system has to be lossless and thus represented by a unitary matrix H. Second, for each camera pixel k that satisfies $|h_{kj}|^2 \neq 0$, the following phase-matching condition needs to be fulfilled:

$$\phi_j + \beta_{kj} - \alpha_k = \pi/2 + m\pi \qquad (12)$$

with $\alpha_k = \arg(E_k^{\mathrm{det}})$ the phase of the field in the camera plane.

Using the same assumptions, an analogue of Eq. (11) can also be derived for the estimation of other parameters. A common application is the estimation of the number of photons absorbed by the object. Absorptive samples can indeed modulate the amplitude of the incident field, and one may want to estimate the set of parameters $n = (n_1, \ldots, n_p)^{\mathsf{T}}$ instead of ϕ. In such cases, we obtain the following chain of inequalities [24]:

$$\mathrm{Var}(\hat{n}_j) \geq [\mathcal{J}^{-1}(n)]_{jj} \geq [\mathcal{J}(n)]_{jj}^{-1} \geq n_j. \qquad (13)$$

The conditions required to saturate these inequalities are essentially the same as those introduced for phase estimations, except that the phase-matching condition now reads

$$\phi_j + \beta_{kj} - \alpha_k = m\pi. \qquad (14)$$

There is an apparent trade-off between phase and absorption estimations: no absorption information is available when phase information is optimally captured by the measurements, and vice versa.

III. PHASE MICROSCOPES WITH AN EXTERNAL REFERENCE

We first study the consequences of this phase-matching condition for phase microscopes with an external reference. In a simple configuration, the incident wave passes through the sample and is imaged onto the camera using an ideal $4f$ system represented by an identity H matrix [Fig. 1(a)]. In the detector plane, the field interferes with a high-intensity external reference beam, whose phase profile can be shaped using a noiseless spatial light modulator (SLM). For the simulations we chose ($|E_k^{\mathrm{ref}}|^2/|E_k^{\mathrm{obj}}|^2 = 100$ in the center of the FOV). The two beams are coupled using a beam splitter with a transmission close to 1 to preserve the unitarity of H. For such a phase microscope the phase-matching condition expressed by Eq. (12) reduces to $\phi_k - \alpha_k = \pi/2 + m\pi$, where $\alpha_k \simeq \arg(E_k^{\mathrm{ref}})$. Thus, if the reference field is a plane wave with a phase that is shifted by $\pi/2$ with respect to the average phase of the object wave (assumed to be 0 for simplicity), the phase-matching condition is fulfilled for a weakly contrasted object ($\phi_j \ll \pi/2$), yielding an optimal precision for phase estimations. However, this strategy cannot be applied to strongly contrasted objects, as typically encountered in cell biology.

In order to test the precision that can be achieved in such cases, we generate a 128×128 complex-valued object with a phase distribution produced from the "cameraman"
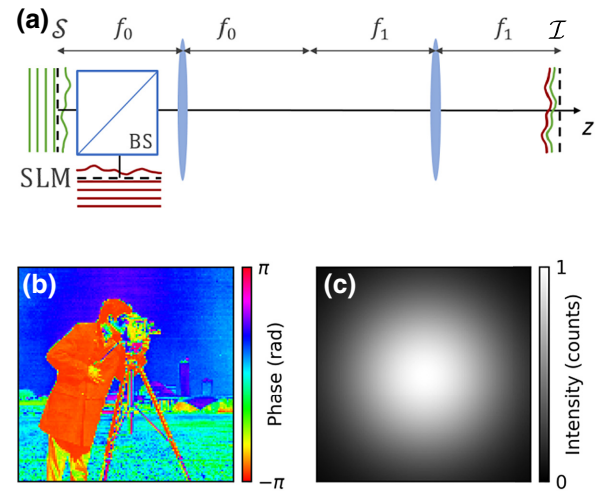

FIG. 1. (a) Schematics of a phase microscope operating with external reference wave. The sample $\mathcal{S}$ is imaged onto the image plane $\mathcal{I}$ using a $4f$ setup. The object wave (green) is interfered with an external reference (red), which is introduced using a beam splitter (BS). The reference wave can be shaped using a spatial light modulator (SLM). (b) Phase of the object wave after interacting with an artificial nonabsorbing sample ranging from $-\pi$ to π. (c) Intensity of the object wave, showing the Gaussian envelope of the incoming beam.
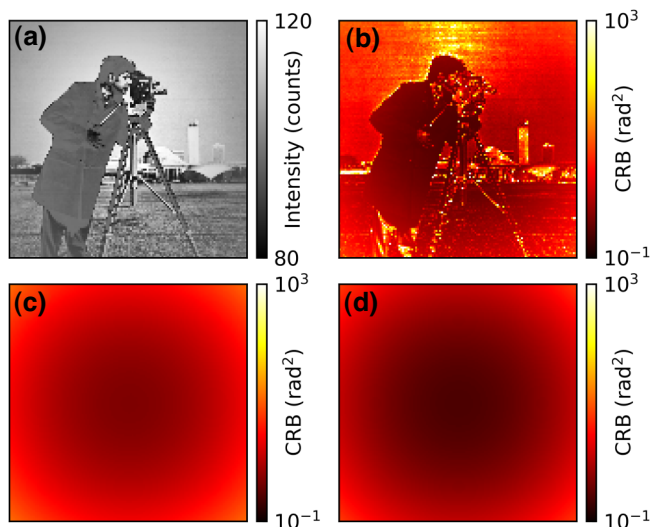
FIG. 2. (a) Simulated intensity in the camera plane for on-axis interferometric imaging with a reference beam that is phase shifted by $\pi/2$, and (b) resulting CRB. (c) CRB for phase-shifting interferometric imaging using four images that are taken with a reference beam that is phase shifted by 0, $\pi/2$, π, and $3\pi/2$. (d) CRB for the optimized scheme: the external reference is shaped according to the sample, such that optimal phase estimation precision is achieved across the FOV.

test image [Fig. 1(b)] and with a Gaussian intensity profile [Fig. 1(c)]. For the calculations, we set the number of photons per frame and unit area n_j to 1 in the center of the Gaussian profile, so that one can easily deduce the CRB for other values of n_j as the CRB scales with $1/n_j$. In Fig. 2(a) we show the simulated intensity distribution in the camera plane. By evaluating partial derivatives of the intensity with respect to each parameter using a finite-difference scheme, the Fisher information matrix can then be calculated according to Eq. (6), as shown in code 1 [25]. The resulting CRB (in rad^2) is shown in Fig. 2(b). In certain regions of the sample in which the phase-matching condition is fulfilled, the optimal precision is reached, resulting in a CRB equal to $1/(4n_j) = 0.25$ rad^2. However, the CRB strongly increases in other regions, in which the phase-matching condition is not fulfilled. We observe that this lower bound on the variance can become much larger than π^2, which means that meaningful estimations of the phase cannot be achieved with $n_j \leq 1$. This has important practical implications: even if $n_j \simeq 10^4$ (as can be achieved with typical complementary metal-oxide-semiconductor detectors), the CRB could be as high as 0.1 rad^2, preventing the high-speed detection of small phase shifts as induced by, e.g., neuronal activity [26] or viral infection [27].

This problem can be addressed with phase-shifting interferometric schemes, in which the object field is successively interfered with $N \geq 3$ reference fields that are phase shifted by $2u\pi/N$, where $u = 0, \ldots, N-1$. As the Fisher information is additive for independent measurements, this

procedure yields an averaging effect, resulting in a CRB equal to $1/(2n_j)$, with an increase by a factor of 2 as compared to the optimal limit [24]. Consequently, the resulting spatial distribution of the CRB is now dictated by the Gaussian distribution of the number of incoming photons, as shown in Fig. 2(c). Note that the same averaging effect can also be achieved with off-axis interferometric imaging [28]. In such a scheme, however, independent measurements for different values of α_k are obtained by oversampling the field in the camera plane instead of by taking several images.

In order to realize optimal phase estimations, the phase-matching condition expressed by Eq. (12) has to be fulfilled throughout the entire FOV. This can be achieved with a SLM by spatially modulating either the reference wave (to modulate α_k) or the object wave (to modulate ϕ_k), yielding the optimal CRB of $1/(4n_j)$ for phase estimations [Fig. 2(d)]. This strategy requires prior knowledge about the object and, at first glance, it may seem of little use to perform an optimal measurement on a known object. In practice, however, coarse knowledge is sufficient to initialize a measurement close to the CRB [24]. The additional number of photons required for coarse initialization is small, and can be neglected in the analysis (especially for continuous measurements, for which initialization is only needed in the beginning of the acquisition). For instance, such an approach is routinely implemented in the context of single-mode interferometry such as in the LIGO experiment in which, apart from shot noise, various other noise sources are taken into account to find the optimal operational point [29]. Starting from an unknown object, an iterative strategy can be devised, thus progressively approaching the optimal precision limit [30].

IV. PHASE MICROSCOPES WITH AN INTERNAL REFERENCE

Techniques based on an external reference are experimentally often limited by vibrations, which lead to an unstable phase difference between reference and object waves. This constraint led to the widespread application of phase microscopy using an internal reference wave in a stable common-path geometry. Already in the 30s, Zernike realized that a wavefront transmitted by a weakly contrasted object can be understood as the superposition of an unscattered plane wave and a scattered wave, which led him to invent phase-contrast microscopy (PCM) [1]. In ordinary PCM, a typically ring- or disc-shaped phase mask is placed in the Fourier plane of the $4f$ imaging system to shift the phase between the scattered and unscattered wave by $\pm\pi/2$ [Fig. 3(a)]. However, while this strategy yields the optimal precision for phase estimations in the case of weakly contrasted objects, this is not the case for strongly contrasted objects. We numerically model PCM by applying a fast Fourier transform algorithm to the phase

object represented in Fig. 1(b) and Fig. 1(c) and by shifting the phase of the central pixel by $\gamma = \pi/2$. The resulting intensity distribution in the camera plane [Fig. 4(a)] and the associated suboptimal CRB [Fig. 4(b)] remarkably differ from the results shown in Figs. 2(a) and 2(b), where we consider an external reference wave shifted by $\pi/2$. Indeed, highly scattering regions deplete the internal reference (i.e., the light passing through the phase mask), making phase measurements highly inefficient. Another important consideration is that, with an internal reference, measurements are insensitive to the global phase of the object wave. Thus, the Fisher information matrix is singular unless this parameter is excluded from its definition. Such consideration is especially important when considering a situation in which spatial frequencies beyond the numerical aperture of the optical system are lost, and in which only absorption information can be accessed for low spatial frequencies that fall within the phase disc [24].

It is instructive to compare these results with imaging schemes that rely on phase stepping. One example is spatial light interference microscopy (SLIM) [20], a scheme that is similar to standard PCM but which includes the option to control the phase shift γ. Several measurements are performed by successively changing the value of γ to 0, $\pi/2$, π, and $3\pi/2$, as implemented in Ref. [20]. While we show that the CRB depends only on the number of incident photons for a phase-shifting interferometric scheme with an external reference [see Fig. 2(c)], this is not the case for an internal reference wave. This can be seen in Fig. 4(c), which shows strong variations in the CRB across
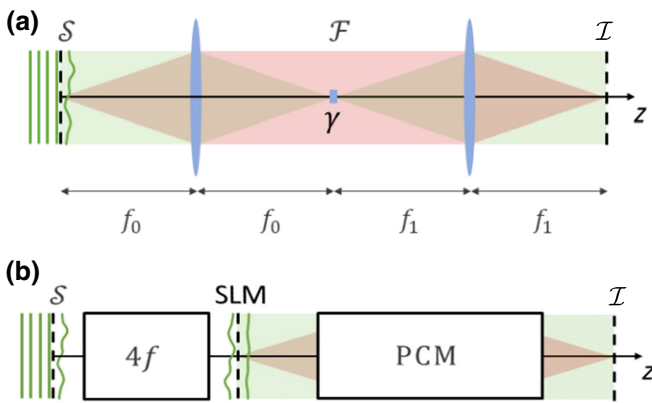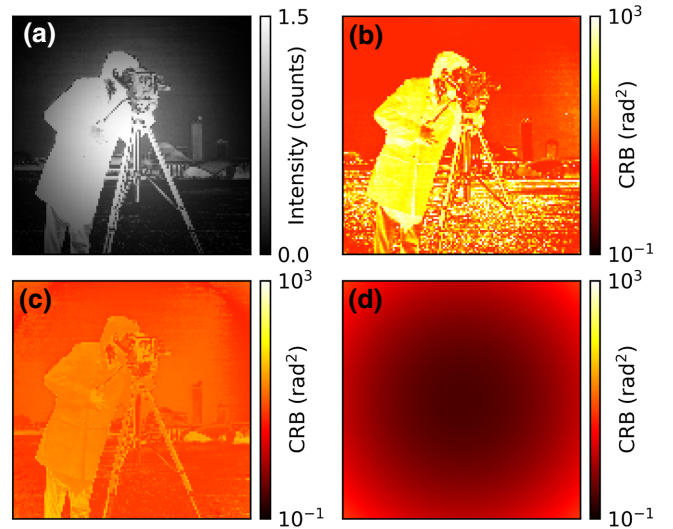

FIG. 4. (a) Simulated intensity in the camera plane for PCM and (b) resulting CRB. (c) CRB for SLIM: four images are taken with an internal reference that is phase shifted by 0, $\pi/2$, π, and $3\pi/2$. (d) CRB for Lowphi: a SLM is used to subtract an estimated phase distribution from the object wave, such that optimal phase estimation precision is achieved across the FOV.

the FOV. This effect is again due to a depletion of the internal reference for strongly scattering regions, as already discussed in our analysis of PCM.

This problem can be addressed using a recent method called local optimization of wavefronts for phase imaging (LowPhi) [23]. In this scheme, the object is imaged onto a SLM and the resulting wavefront is then imaged using traditional PCM [Fig. 3(b)]. The system is first initialized, such that the SLM approximately cancels phase variations induced by the object. If the error in the initialization is small then the following PCM is an optimal measurement scheme for these deviations. In Fig. 4(d) we show the resulting CRB, which is indeed optimal over the entire FOV. This demonstrates that one does not need an external reference beam [as considered in Fig. 2(d)] to reach the optimal precision for phase estimations. In both cases, however, optimal phase estimations come at the price of the required initialization (the photon budget of which can be neglected for continuous measurements) and technical issues regarding SLM phase noise [31]. Moreover, measurements are then fully insensitive to the amplitude of the object wave, and one would have to replace the PCM after the SLM by a standard bright-field microscope in order to perform optimal absorption estimations.

V. CONCLUSION

To summarize, we show that the Cramér-Rao bound is a powerful tool to investigate the estimation precision of phase microscopes. The general framework that we introduce here enables the analysis of any classical phase

FIG. 3. (a) Schematics of phase contrast microscopy (PCM). The sample $\mathcal{S}$ is imaged onto the image plane $\mathcal{I}$ using a modified $4f$ setup, in which the unscattered light (green) is phase shifted by an angle γ with respect to the scattered light (red). For ordinary PCM, the phase shift is realized in the Fourier plane $\mathcal{F}$ and its value is set to $\gamma = \pm\pi/2$. (b) Schematics of a LowPhi setup. The sample $\mathcal{S}$ is imaged onto a SLM using a $4f$ setup (note that the order could be reversed). The SLM is used to subtract an estimated phase distribution from the object wave, which is then imaged using the PCM scheme shown above.

microscope that can be described by a linear transformation. This allows one to assess whether a chosen technique can in principle provide the precision required for challenging tasks, such as the high-speed detection of small phase shifts induced by neuronal activity [26] or viral infection [27]. It can also allow one to verify whether the precision of phase estimates is limited by shot noise, or whether this precision is degraded by additional noise sources (e.g., due to mechanical instabilities) that could easily be described using the same formalism.

Importantly, our analysis yields the necessary conditions for reaching the optimal precision in phase estimations (as well as those needed to perform optimal absorption estimations). A critical requirement for reaching the optimal phase precision is a phase-matching condition between object wave and reference wave, which can either be internal or external. With this theoretical framework, we analyze the precision achievable with different experimental configurations, evidencing that wavefront shaping can enable optimal phase (or absorption) estimation precision, even in the absence of an external reference wave (e.g., in LowPhi [23]). In practice, such approaches based on wavefront shaping are currently limited by SLM phase noise, therefore requiring alternative approaches to phase microscope optimization based on, e.g., generalized phase contrast [32] or deep learning [33]. Interestingly, these alternative approaches could also be benchmarked using the Cramér-Rao analysis presented here.

Further work will be needed to assess the performance of minimum variance unbiased estimators relative to these bounds, and to perform experimental measurements with a precision reaching the theoretical limit. Finally, note that the formalism can be extended to schemes that further improve the precision of phase microscopy using cavities [34,35], and can also be applied to electron phase microscopy techniques [36,37].

See the Supplemental Material for supporting content [24]. The PYTHON code for this project is given in Ref. [25].

ACKNOWLEDGMENTS

[1] F. Zernike, Phase contrast: A new method for the microscopic observation of transparent objects, Physica **9**, 686 (1942).

[2] D. Gabor, A new microscopic principle, Nature **161**, 777 (1948).

[3] G. Popescu, *Quantitative Phase Imaging of Cells and Tissues* (McGraw-Hill, New York, 2011).

[4] K. R. Lee, K. Kim, J. Jung, J. H. Heo, S. Cho, S. Lee, G. Chang, Y. J. Jo, H. Park, and Y. K. Park, Quantitative phase imaging techniques for the study of cell pathophysiology: From principles to applications, Sensors (Switzerland) **13**, 4170 (2013).

[5] M. R. Andrews, M.-O. Mewes, N. J. van Druten, D. S. Durfee, D. M. Kurn, and W. Ketterle, Direct, nondestructive observation of a Bose condensate, Science **273**, 84 (1996).

[6] P. J. Windpassinger, D. Oblak, P. G. Petrov, M. Kubasik, M. Saffman, C. L. G. Alzar, J. Appel, J. H. Müller, N. Kjærgaard, and E. S. Polzik, Nondestructive Probing of Rabi Oscillations on the Cesium Clock Transition near the Standard Quantum Limit, Phys. Rev. Lett. **100**, 103601 (2008).

[7] A. Ojaghi, M. E. Fay, W. A. Lam, and F. E. Robles, Ultraviolet hyperspectral interferometric microscopy, Sci. Rep. **8**, 1 (2018).

[8] M. C. Cheung, R. LaCroix, B. K. McKenna, L. Liu, J. Winkelman, and D. J. Ehrlich, Intracellular protein and nucleic acid measured in eight cell types using deep-ultraviolet mass mapping, Cytometry A **83**, 540 (2013).

[9] H. L. V. Trees, K. L. Bell, and Z. Tian, *Detection Estimation and Modulation Theory, Part I* (John Wiley & Sons, Hoboken, New Jersey, 2013).

[10] H. H. Barrett and K. J. Myers, *Foundations of Image Science* (John Wiley & Sons, Hoboken, New Jersey, 2013).

[11] H. Deschout, F. C. Zanacchi, M. Mlodzianoski, A. Diaspro, J. Bewersdorf, S. T. Hess, and K. Braeckmans, Precisely and accurately localizing single emitters in fluorescence microscopy, Nat. Methods **11**, 253 (2014).

[12] Y. Shechtman, S. J. Sahl, A. S. Backer, and W. Moerner, Optimal Point Spread Function Design for 3D Imaging, Phys. Rev. Lett. **113**, 133902 (2014).

[13] F. Balzarotti, Y. Eilers, K. C. Gwosch, A. H. Gynnå, V. Westphal, F. D. Stefani, J. Elf, and S. W. Hell, Nanometer resolution imaging and tracking of fluorescent molecules with minimal photon fluxes, Science **355**, 606 (2017).

[14] M. Piliarik and V. Sandoghdar, Direct optical sensing of single unlabelled proteins and super-resolution imaging of their binding sites, Nat. Commun. **5**, 1 (2014).

[15] D. Bouchet, R. Carminati, and A. P. Mosk, Influence of the Local Scattering Environment on the Localization Precision of Single Particles, Phys. Rev. Lett. **124**, 133903 (2020).

[16] P. C. Doerschuk and J. E. Johnson, Ab initio reconstruction and experimental design for cryo electron microscopy, IEEE Trans. Inf. Theory **46**, 1714 (2000).

[17] P. C. Humphreys, M. Barbieri, A. Datta, and I. A. Walmsley, Quantum Enhanced Multiple Phase Estimation, Phys. Rev. Lett. **111**, 070403 (2013).

[18] J. Liu, H. Yuan, X. M. Lu, and X. Wang, Quantum Fisher information matrix and multiparameter estimation, J. Phys. A Math. Theor. **53**, 023001 (2020).

[19] C. Maurer, A. Jesacher, S. Bernet, and M. Ritsch-Marte, What spatial light modulators can do for optical microscopy, Laser Photon. Rev. **5**, 81 (2011).

[20] Z. Wang, L. Millet, M. Mir, H. Ding, S. Unarunotai, J. Rogers, M. U. Gillette, and G. Popescu, Spatial light interference microscopy (SLIM), Opt. Express **19**, 1016 (2011).

[21] K. Toda, M. Tamamitsu, and T. Ideguchi, Adaptive dynamic range shift (ADRIFT) quantitative phase imaging, Light Sci. Appl. **10**, 1 (2021).

[22] D. Bouchet, S. Rotter, and A. P. Mosk, Maximum information states for coherent scattering measurements, Nat. Phys. (2021).

[23] T. Juffmann, A. de los Ríos Sommer, and S. Gigan, Local optimization of wave-fronts for optimal sensitivity PHase imaging (LowPhi), Opt. Commun. **454**, 124484 (2020).

[24] See Supplemental Material at http://link.aps.org/supplemental/10.1103/PhysRevApplied.15.024047 for additional considerations on absorption estimation, phase-shifting interferometry, incomplete knowledge of phase objects, and singularity of the Fisher information matrix.

[25] D. Bouchet, J. Dong, D. Maestre, and T. Juffmann, Python code for Cramér-Rao analysis of phase microscopy techniques (2021), https://github.com/JuffmannLab/PhaseMicroscopyCRB.

[26] T. Ling, K. C. Boyle, G. Goetz, P. Zhou, Y. Quan, F. S. Alfonso, T. W. Huang, and D. Palanker, Full-field interferometric imaging of propagating action potentials, Light Sci. Appl. **7**, 107 (2018).

[27] Y. F. Huang, G. Y. Zhuo, C. Y. Chou, C. H. Lin, W. Chang, and C. L. Hsieh, Coherent brightfield microscopy provides the spatiotemporal resolution to study early stage viral infection in live cells, ACS Nano **11**, 2575 (2017).

[28] E. N. Leith and J. Upatnieks, Wavefront reconstruction with continuous-tone objects, J. Opt. Soc. Am. **53**, 1377 (1963).

[29] C. Bond, D. Brown, A. Freise, and K. A. Strain, *Living Reviews in Relativity* (Springer International Publishing, 2016), Vol. 19, p. 1.

[30] B. L. Higgins, D. W. Berry, S. D. Bartlett, H. M. Wiseman, and G. J. Pryde, Entanglement-free Heisenberg-limited phase estimation, Nature **450**, 393 (2007).

[31] S. Moser, M. Ritsch-Marte, and G. Thalhammer, Model-based compensation of pixel crosstalk in liquid crystal spatial light modulators, Opt. Express **27**, 25046 (2019).

[32] J. Glückstad and D. Palima, Generalized phase contrast, Springer Ser. Opt. Sci. **146**, 7 (2009).

[33] M. R. Kellman, E. Bostan, N. A. Repina, and L. Waller, Physics-based learned design: Optimized coded-illumination for quantitative phase imaging, IEEE Trans. Comput. Imaging **5**, 344 (2019).

[34] S. Nimmrichter, C.-F. Chen, B. B. Klopfer, M. A. Kasevich, and T. Juffmann, Full-field cavity enhanced microscopy techniques, J. Phys. Photonics **1**, 015007 (2019).

[35] M. Mader, J. Reichel, T. W. Hänsch, and D. Hunger, A scanning cavity microscope, Nat. Commun. **6**, 7249 (2015).

[36] R. Danev and W. Baumeister, Expanding the boundaries of cryo-EM with phase plates, Curr. Opin. Struct. Biol. **46**, 87 (2017).

[37] C. Ophus, J. Ciston, J. Pierce, T. R. Harvey, J. Chess, B. J. McMorran, C. Czarnik, H. H. Rose, and P. Ercius, Efficient linear phase contrast in scanning transmission electron microscopy with matched illumination and detector interferometry, Nat. Commun. **7**, 1 (2016).